The Ion Temperature Gradient Contribution to the Global Magnetopause Current

J. M. H. Beedle[1,2], D. J. Gershman[2], V. M. Uritsky[1,2], T. D. Phan[3], B. L. Giles[2]

[1]Department of Physics, The Catholic University of America, Washington D.C. USA
[2]NASA Goddard Space Flight Center, Greenbelt, MD, USA
[3]Space Sciences Laboratory, University of California, Berkeley, CA, USA

Key Points:

- The ion temperature gradient generates up to 30% of the diamagnetic current along the magnetopause
- The temperature gradient current component typically opposes the classical Chapman-Ferraro current direction
- The temperature component has a larger impact on the flank magnetopause

Corresponding author: Jason Beedle, `beedle@cua.edu`

Abstract

Magnetopause diamagnetic currents arise from density and temperature driven pressure gradients across the boundary layer. While theoretically recognized, the temperature contributions to the magnetopause current system have not yet been systematically studied. To bridge this gap, we used a database of Magnetospheric Multiscale (MMS) magnetopause crossings to analyze diamagnetic currents and their contributions across the dayside and flank magnetopause. Our results indicate that the ion temperature gradient component makes up to 30% of the ion diamagnetic current along the magnetopause and typically opposes the classical Chapman-Ferraro current direction, interfering destructively with the density gradient component, thus lowering the total diamagnetic current. This effect is most pronounced on the flank magnetopause. The electron diamagnetic current was found to be 4 to 12 times weaker than the ion diamagnetic current on average.

Plain Language Summary

The solar wind represents a continuous outflow of charged particles from the Sun's upper atmosphere into the solar system. Upon reaching Earth's magnetosphere, the solar wind's dynamic pressure is balanced by the magnetic pressure of Earth's magnetic field in a boundary layer known as the magnetopause. This boundary layer represents the entry point of the solar wind's energy into Earth's magnetosphere and upper atmosphere, playing a crucial role in energy transport throughout the interconnected system. Plasma density and temperature differences across the boundary layer generate an electric current that supports the magnetopause. In this paper, we clarify the physical mechanism of the magnetopause current by using high-resolution data from NASA's MMS mission. We found a significant ion temperature contribution to the magnetopause current not identified in previous studies. Our results also indicated that the plasma electrons' contribution to the magnetopause current was significantly smaller than the ion contribution.

1 Introduction

The magnetopause is a magnetosphere boundary layer created through the dynamic pressure balance between the solar wind's kinetic pressure and Earth's magnetic field. The solar wind causes distortions in the magnetosphere's magnetic field topology supported by a current sheet first proposed by Chapman and Ferraro in 1931 (Chapman & Ferraro, 1931), often termed the Chapman-Ferraro (CF) current, which runs in a dawn-to-dusk direction around the magnetopause (Ganushkina et al., 2018). This current structure is believed to be generated through pressure gradients at the magnetopause boundary layer where, as explained in Hasegawa (2012), the magnetosheath plasma has a higher plasma density, while the magnetosphere will have a higher ion temperature. The resulting changes in plasma density and temperature across the magnetopause leads to gradients that generate ion and electron diamagnetic currents running perpendicular to the magnetic field (Ganushkina et al., 2018).

Because of the magnetopause's important role in magnetic reconnection and the resulting transfer of plasma and energy into the magnetosphere it has been the focus of numerous studies [Cahill and Amazeen (1963); Le and Russell (1994); Phan et al. (1996); Phan and Paschmann (1996); Haaland et al. (2014); Paschmann et al. (2018); Haaland et al. (2019); Shuster et al. (2019); Haaland et al. (2020); etc.] and missions [MMS, THEMIS, and Cluster] which have delved deeper into the current sheet's structure and creation. From Paschmann et al. (2018) and their MMS magnetopause crossing database, the total current density across the dayside magnetopause was studied in detail. The flank magnetopause total current density was then surveyed in Haaland et al. (2019) and Haaland

et al. (2020) where the flanks were found to have a weaker current density and a correspondingly thicker boundary layer than the dayside.

While the literature generally recognizes the importance of both the density and temperature in generating diamagnetic currents, a large scale systematic analysis of the temperature gradient's impact on the magnetopause current system has not yet been accomplished. To help fill this gap in the literature, we considered four years of burst mode MMS mission data over the magnetopause crossing intervals provided by Paschmann et al. (2018)'s MMS database. This allowed us to study the diamagnetic current and specifically focus on the component generated from the divergence of the ion temperature to measure its impact across the magnetopause. We measured both the density and temperature diamagnetic current components and created current accumulations of their contributions. In doing so, we found that the temperature diamagnetic current component is an important factor to both the dayside and flank magnetopause current sheet by acting against the density component and reducing its impact.

2 Data and Analysis

2.1 MMS Database

For this study, we used four years of data from Paschmann et al. (2018, 2020)'s and Haaland et al. (2020)'s database of MMS current sheet crossings. MMS is a mission comprised of four separate spacecraft traveling in a tetrahedron pattern through the magnetopause (Burch et al., 2015). This database catalogues MMS current sheet crossings based on Fast Plasma Investigation (FPI) (Pollock et al., 2016), Fluxgate Magnetometer (Russell et al., 2016), and Hot Plasma Composition Analyzer (HPCA) measurements (Young et al., 2016). The magnetopause transit times are captured through minimum variance analysis of the magnetic field in boundary normal or LMN coordinates (Paschmann et al., 2018, 2020). The database then places identifiers on individual magnetopause crossings classifying their characteristics and structure. A full description of this process and the current sheet identifiers can be found in Paschmann et al. (2018).

We chose 767 magnetopause crossings from 2015 to 2018 using database event identifiers to select for complete, monotonic, magnetopause crossings, where monotonic indicated events that had a constant magnetopause velocity so their thicknesses and durations could be computed using the methods described by Sonnerup and Wang (1987). Additionally, we included Harris sheet-like events, or simple clear magnetopause crossings that were also complete, monotonic events in our data set. Events with unusually high (above $2,000\ nA/m^2$) diamagnetic current spikes during the magnetopause crossing time, such as would occur during a reconnection event, or when data flags for the various instruments were non-nominal, were manually removed from our data set. The locations and corresponding years of the 767 selected crossings are denoted in Figure 1.

As an added condition, we used the HPCA to compare the number densities of H^+ with O^+ for each magnetopause crossing. If O^+ exceeded 0.2 cm^{-3} during the transit and H^+ remained below 1.5 cm^{-3}, then we considered O^+ to dominate the magnetospheric ion mass density by more than a factor of 2 as described by Fuselier et al. (2019). Events fitting this classification were also removed from our data set as they represented densities not typically found in the magnetopause current sheet.

2.2 Current Calculations

MMS's four separate spacecraft allows the total current to be calculated by the curlometer method (Dunlop et al., 1988) that uses all four spacecraft to perform the curl of the observed magnetic field in order to approximate Ampere's law in the MHD approximation. This current we call the curlometer current:

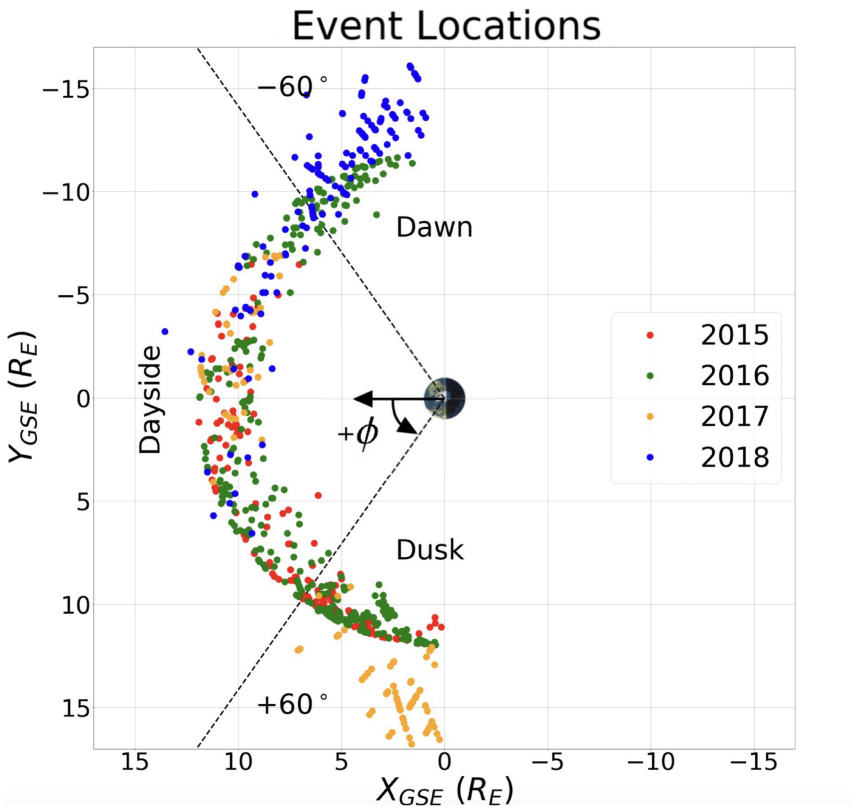

Figure 1. Diagram of the 767 MMS magnetopause crossings from 2015 (red), 2016 (green), 2017 (orange), and 2018 (blue) used in our study. We define a local spherical coordinate system with ϕ in the X_{GSE} - Y_{GSE} plane, positively defined from the $+X_{GSE}$ axis, R defined as radially outward, and θ as the azimuthal angle into the Z_{GSE} direction. Note, every 15° in ϕ is equal to 1 hour of MLT with 12 MLT corresponding to 0° in ϕ, or along the $+X_{GSE}$ axis. The Dawn flank is then defined between −60° and −90° in ϕ, the Dusk flank between +60° and +90°, and the Dayside is defined from +60° and −60°. This magnetopause breakdown is adopted from the approach taken by Haaland et al. (2020). Note, MMS first launched in 2015 with an orbit focusing on the dayside magnetopause, but after 2017, this orbit was extended to a wider orbit focusing on the flank magnetopause (Haaland et al., 2020). Thus the dusk transits are biased toward 2015, 2016, and 2017 measurements, while the dawn transits are mainly composed of 2016 and 2018 measurements. Because of the varying solar cycle, this has the possibility of creating an asymmetry between the dawn and dusk flank plasma measurements.

$$\mathbf{J}_{curl} \approx \frac{\nabla \times \mathbf{B}}{\mu_0}. \tag{1}$$

Using the curlometer method, we also calculated the gradient of the ion density, and the divergence of the temperature tensor to get the total ion diamagnetic current and its current components ($\mathbf{J}_{dia\ \nabla N_i}$ and $\mathbf{J}_{dia\ \nabla\cdot\overleftrightarrow{T_i}}$). We found the electron diamagnetic current to be at least one order of magnitude smaller, on average, than the ion diamagnetic current. This is in agreement with the results of Dong et al. (2018) in their case study where they found that the perpendicular current was mainly carried by the ion diamagnetic current in the magnetopause. Thus we are presenting results for the ion components and will drop the signifier "i" going forward. The components and the total perpendicular diamagnetic current are then defined as follows:

$$\mathbf{J}_{dia\ \nabla N} = \frac{\mathbf{B} \times (K_b \overleftrightarrow{T} \cdot \nabla N)}{|\mathbf{B}|^2} \quad , \quad \mathbf{J}_{dia\ \nabla\cdot\overleftrightarrow{T}} = \frac{\mathbf{B} \times (K_b N \nabla \cdot \overleftrightarrow{T})}{|\mathbf{B}|^2}. \tag{2}$$

Where $\mathbf{J}_{dia\ Total} = \mathbf{J}_{dia\ \nabla N} + \mathbf{J}_{dia\ \nabla\cdot\overleftrightarrow{T}}$.

We also considered the total parallel current or $J_{\parallel} = \frac{(B \cdot J_{curl})B}{|B^2|}$.

All of the data taken from MMS, as well as the current calculations, was interpolated to the 30 ms FPI electron time resolution. As our main results involve ion diamagnetic currents and the total current as computed from the curlometer method, any sub 150 ms variations in the ion measurements will not impact our results. For non-curlometer calculations, we averaged over all four spacecraft to create a single data stream where, on average, the MMS separation during 2015 - 2018 was 10 - 60 km while the magnetopause current crossings analyzed typically had thicknesses greater than several hundred km, sufficiently larger than the max 60 km tetrahedron separation. These calculations were completed in GSE coordinates and then converted to a local spherical coordinate system built off of the Cartesian GSE coordinates. See Figure 1 for a depiction of our spherical coordinate system and the definition of the dusk and dawn sectors.

2.3 Current Sheet Identification

From the database, we are provided with the deHoffman-Teller (HT) boundaries (Sonnerup & Wang, 1987) of each event given as a 100% extension of the database defined magnetopause crossings (Paschmann et al., 2018). Through visual analysis, we found that the majority of the database's HT time frames contained magnetic, plasma, and current signatures consistent with a magnetopause crossing; however, the database's automatically assigned magnetopause crossing times, based on minimum variance analysis of the magnetic field, often did not provide a good match with these signatures. This discrepancy is not unexpected given that the magnetic field is not enough, by itself, to select a magnetopause crossing. Instead, the magnetopause can be described as a boundary where the magnetic field intensity changes over a current layer as reiterated in Hasegawa (2012). We thus created a new parameter to capture significant, continuous current segments, without biasing toward brief current spikes, during magnetic field fluctuations in the database's HT boundaries for each individual event.

To accomplish this over our subset of database crossings, we looked at the curlometer current during each event's HT time frame. $\mathbf{J}_{curl}$ was then smoothed and separated into current segments by applying a dynamic threshold equal to 15% of the maximum $\mathbf{J}_{curl}$ value for that specific crossing. Each segment began once the current passed this threshold and ended once the current dipped below. We utilized a dynamic threshold in order to better capture a wide range of current structures as the database included

events with vastly different solar wind driving conditions. See Figure 2g for an example of a current segment, represented between the orange dashed lines.

Over each segment, we recorded three quantities: the average curlometer current ($\mathbf{J}_{curl\ avg}$), the length of the segment (L), and the change in $|\mathbf{B}|$ ($\Delta\mathbf{B}$). For a given magnetopause crossing, the identified current segments were compared with one another and the maximum segment values for $\mathbf{J}_{curl\ avg}$, L, and $\Delta\mathbf{B}$ located. We then divided each segment's quantities by the maximum values to create dimensionless ratios normalized to 1. The ratios are defined as follows:

$$\alpha = \frac{\mathbf{J}_{curl\ avg}}{\mathbf{J}_{curl\ avg\ max}} \quad , \quad \gamma = \frac{L}{L_{max}} \quad , \quad \delta = \frac{\Delta\mathbf{B}}{\Delta\mathbf{B}_{max}} \tag{3}$$

These ratios then form a quality factor (η) to rate the relevance of a current segment during an event's HT time frame. We weighted the ratios based on visual inspection with the following weights:

$$\eta = 0.50\ \alpha + 0.25\ \gamma + 0.25\ \delta. \tag{4}$$

The maximum value for η is held by the segment that has the largest change in the magnetic field, the longest length, and the highest average current density, giving a value of 1. The current segment with the highest resulting η was then selected as the magnetopause current sheet crossing.

This method was visually confirmed for many magnetopause crossings. See Figure 2 for an example of the magnetopause selection process. The currents and other values were then averaged over the selected magnetopause crossings (between the orange dashed lines in Figure 2) for each magnetopause crossing event.

2.4 Current Accumulations

The averaged currents from the 767 magnetopause crossings were put into bins corresponding to MMS's physical location in our local spherical coordinate system. The angle ϕ was used to create 1-dimensional bins from 90° to −90° in 20° increments. This was done for each component in the spherical coordinate system as described in Figure 1 and shown in Figure 3. Error bars for each figure were computed using the standard error or $\sigma/\sqrt{N}$, with σ the standard deviation of the values in each bin and N the number of events that fell inside that bin.

Using Figure 3 we can make several observations. The first is that the $\mathbf{J}_{curl}$, $\mathbf{J}_{dia\ Total}$, and $\mathbf{J}_{dia\ \nabla N}$ ϕ-component currents are all in the $+\phi$ direction across the magnetopause, or in the classical CF, dawn-to-dusk direction. However, the $\mathbf{J}_{dia\ \nabla\cdot\overleftrightarrow{T}}$ ϕ component is consistently in the $-\phi$ direction, or from dusk-to-dawn across the magnetopause. Therefore the two components of the ion diamagnetic current, $\mathbf{J}_{dia\ \nabla N}$ and $\mathbf{J}_{dia\ \nabla\cdot\overleftrightarrow{T}}$, are oppositely directed across the magnetopause as can be seen in Figure 3b. The directions of these components are as expected when using the magnetospheric quantities evaluated by Hasegawa (2012) where the density component should run in the traditional CF current direction as the plasma density is higher in the magnetosheath and lower in the magnetosphere. At the same time, it is expected that the ion temperature is lower in the magnetosheath and higher in the magnetosphere, leading to the ion temperature component typically running counter to the CF current direction. On average, however, $\mathbf{J}_{dia\ \nabla N}$ is stronger than $\mathbf{J}_{dia\ \nabla\cdot\overleftrightarrow{T}}$, which allows the total diamagnetic current, $\mathbf{J}_{dia\ Total}$, to still flow in the classical CF direction.

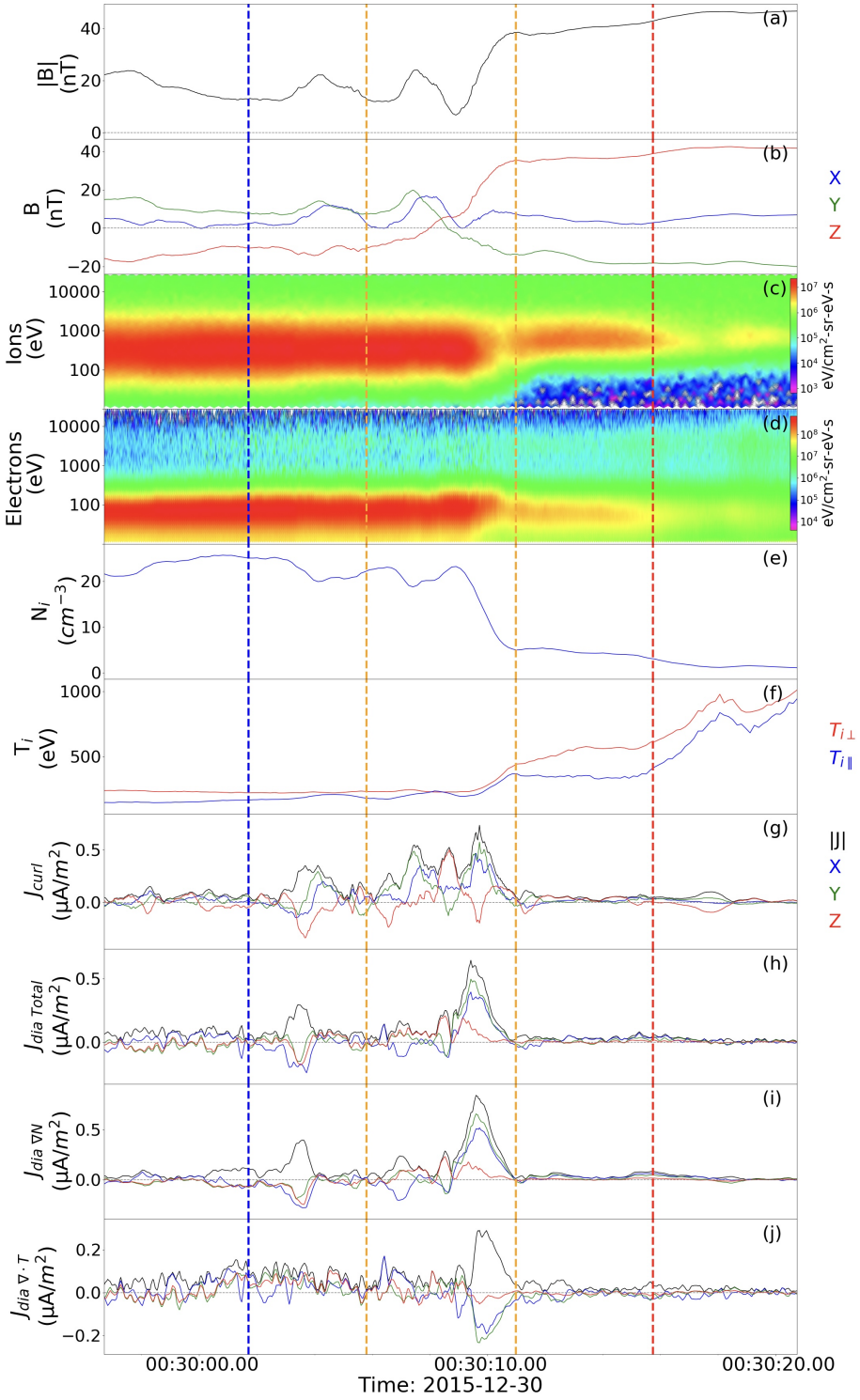

Figure 2. Example crossing during a monotonic, complete 2015 MMS transit from the magnetosheath into the magnetosphere on the dayside magnetopause. The blue and red dashed lines represent the start and the end of the HT time frame as given by the database. The orange lines represent the magnetopause current sheet identified by our thresholding and weighting process.

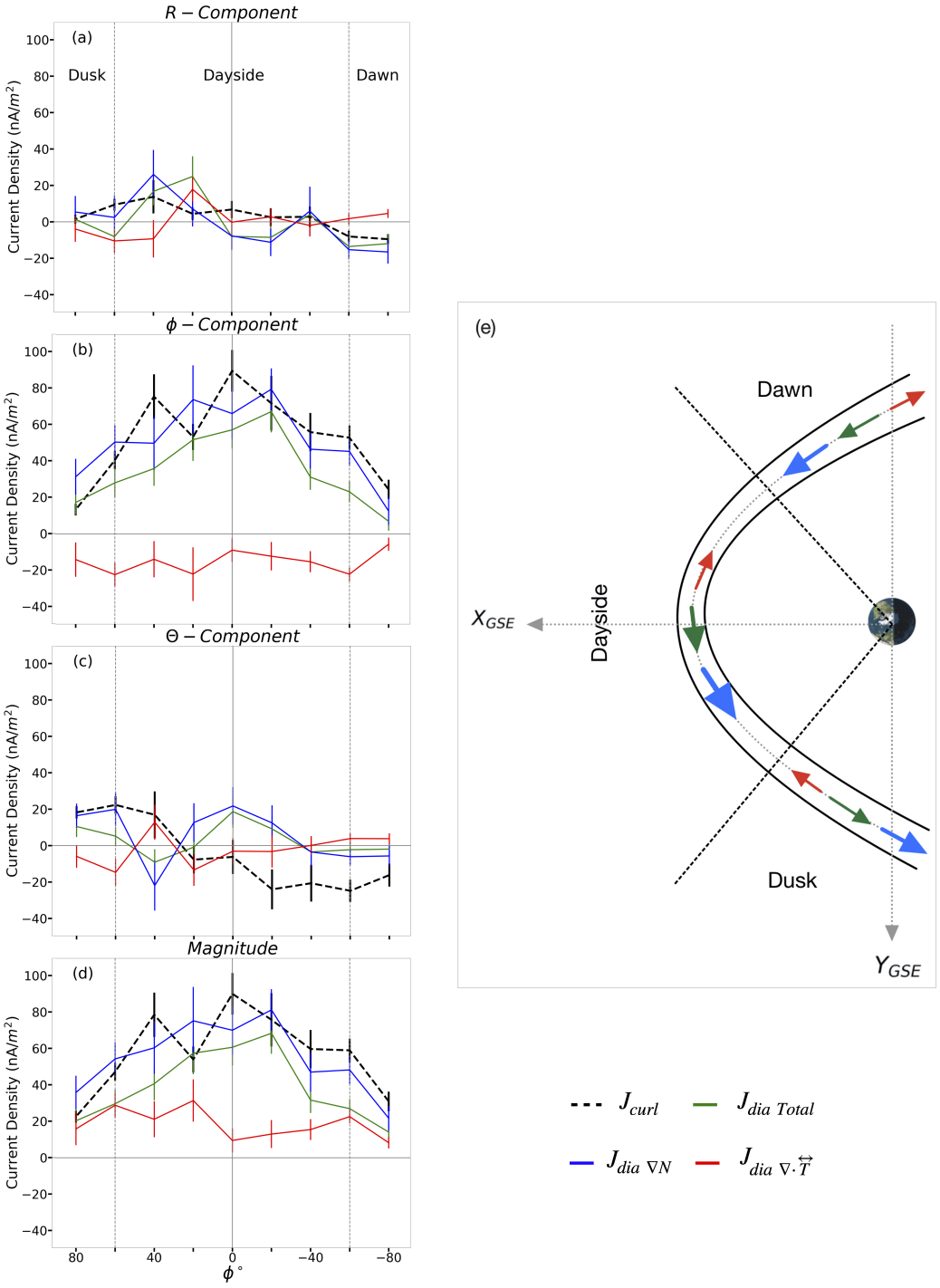

Figure 3. a) through d) depict current density accumulations for $\mathbf{J}_{curl}$, $\mathbf{J}_{dia\ Total}$, $\mathbf{J}_{dia\ \nabla N}$, and $\mathbf{J}_{dia\ \nabla\cdot\overleftrightarrow{T}}$ across the dayside and flank magnetopause sectors, represented by the grey dashed lines. Moving from top to bottom: a). represents the R-component of the current in our local spherical coordinate system (described in Figure 1). b). ϕ - component, c). θ - component, d). magnitude of the current components. e) diagram of the contributions and directions of $\mathbf{J}_{dia\ Total}$, $\mathbf{J}_{dia\ \nabla N}$, and $\mathbf{J}_{dia\ \nabla\cdot\overleftrightarrow{T}}$ across the dusk, dayside, and dawn magnetopause. Note the size of the arrows in each sector indicates the relative magnitude of their current densities and the direction indicates the current component's flow around the magnetopause.

2.5 Current Measurement Results

We used our data to create a table of results over the dusk, dayside, and dawn magnetopause including the mean, median, and standard errors for our 767 magnetopause crossings as seen in Table 1. From these results, the magnetopause is found to be thicker toward the flanks and thinner on the dayside, mirroring the results of Haaland et al. (2020). Additionally, $\mathbf{J}_{curl}$ is strongest on the dayside, with a dusk-dawn asymmetry as the dawn curlometer current is stronger than the dusk. Both $\mathbf{J}_{dia\ Total}$ and $\mathbf{J}_{dia\ \nabla N}$ show similar distributions with the dayside again being the strongest sector, but the dusk and dawn results are now in agreement within their standard errors. Unlike the other currents and current components, $\mathbf{J}_{dia\ \nabla\cdot\overleftrightarrow{T}}$ is almost unchanged across the magnetopause with the dusk, dayside, and dawn values overlapping within the standard errors. The parallel current, $\mathbf{J}_{\parallel}$, is weakest on the dusk, with the dayside and dawn results overlapping within the standard error. The total electron diamagnetic current, $\mathbf{J}_{e\ dia\ Total}$, is the weakest current component studied and shows a dusk-dawn asymmetry with the dawn being stronger than the dusk and the dayside having the largest current density.

Table 1. Magnetopause parameters and current sheet densities across the Dusk, Dawn, and Dayside with the following format: mean (median) ± standard error

Parameter	Dusk	Dayside	Dawn
Number of Crossings	257	384	126
Thickness (km)	1154.6 (792.7) ± 77.7	1115.9 (634.2) ± 79.5	1188.9 (842.1) ± 111.7
Thickness (d_i)	12.7 (8.9) ± 0.8	15.2 (8.8) ± 1.1	16.2 (10.7) ± 1.6
Thickness (R_{gi})	23.4 (10.1) ± 3.0	45.6 (14.2) ± 5.3	20.4 (11.4) ± 3.2
V_n (km/s)	129.4 (109.8) ± 6.2	95.9 (70.9) ± 5.2	96.1 (89.5) ± 5.4
Duration (s)	9.7 (7.4) ± 0.5	11.9 (9.4) ± 0.5	12.1 (9.3) ± 0.7
$\lvert\mathbf{J}_{curl}\rvert$ (nA/m^2)	28.0 (13.3) ± 3.6	65.6 (48.2) ± 4.5	41.2 (17.2) ± 6.2
$\lvert\mathbf{J}_{dia\ Total}\rvert$ (nA/m^2)	19.6 (9.2) ± 6.8	44.9 (30.6) ± 4.7	20.8 (12.7) ± 4.3
$\lvert\mathbf{J}_{dia\ \nabla N}\rvert$ (nA/m^2)	37.1 (20.8) ± 9.0	61.5 (42.8) ± 6.8	34.1 (25.3) ± 6.0
$\lvert\mathbf{J}_{dia\ \nabla\cdot\overleftrightarrow{T}}\rvert$ (nA/m^2)	18.7 (10.6) ± 8.0	16.9 (8.4) ± 4.5	14.0 (9.1) ± 3.1
$\lvert\mathbf{J}_{\parallel}\rvert$ (nA/m^2)	16.9 (5.2) ± 2.9	29.7 (13.9) ± 3.9	24.4 (5.7) ± 5.2
$\lvert\mathbf{J}_{e\ dia\ Total}\rvert$ (nA/m^2)	1.6 (0.5) ± 0.6	4.8 (3.1) ± 0.8	4.2 (2.4) ± 0.6
$T_{i\perp}$ (eV)	872.6 (697.2) ± 38.5	544.3 (474.1) ± 15.1	403.7 (355.4) ± 20.1
N_i (cm^{-3})	9.0 (7.4) ± 0.4	13.8 (11.0) ± 0.5	12.0 (10.1) ± 0.6
B (nT)	16.7 (15.7) ± 0.8	21.5 (20.0) ± 0.8	14.1 (15.4) ± 1.0

3 Temperature Gradient's Impact on the Magnetopause Current System

Using our results from Figure 3 and Table 1, we can posit three primary ways the ion temperature gradients impact the magnetopause current system and, in doing so, create a 2D diagram to summarize our findings as shown in Figure 3e.

1. The divergence of the ion temperature tensor generates up to one third of the total ion diamagnetic current in the ϕ direction.

   Specifically, in the ϕ direction, $\mathbf{J}_{dia\ \nabla\cdot\overleftrightarrow{T}}$ makes up 31% of the diamagnetic current on the dawn, 21% on the dayside, and 33% on the dusk.

2. $\mathbf{J}_{dia\ \nabla\cdot\overleftrightarrow{T}}$ goes in the opposite direction of the classical Chapman-Ferraro Current.

   $\mathbf{J}_{dia\ \nabla\cdot\overleftrightarrow{T}}$ is clearly in the $-\phi$ direction across the magnetopause when considering Figure 3b. This results in $\mathbf{J}_{dia\ \nabla\cdot\overleftrightarrow{T}}$ lowering the contribution of $\mathbf{J}_{dia\ \nabla N}$, making the $\mathbf{J}_{dia\ Total}$ less than $\mathbf{J}_{curl}$ on average as seen in Table 1.

3. $\mathbf{J}_{dia\ \nabla\cdot\overleftrightarrow{T}}$'s contribution to the magnetopause current system becomes more important toward the flank magnetopause.

   $\mathbf{J}_{dia\ Total}$ and $\mathbf{J}_{dia\ \nabla N}$ are strongest on the dayside and grow steadily weaker on the dusk and the dawn flanks, with both flanks showing similar results for the current densities. This is in contrast to $\mathbf{J}_{dia\ \nabla\cdot\overleftrightarrow{T}}$ which stays roughly constant regardless of sector. Thus $\mathbf{J}_{dia\ \nabla\cdot\overleftrightarrow{T}}$ stays constant on the flanks, while $\mathbf{J}_{dia\ \nabla N}$ decreases in strength, resulting in the total diamagnetic current being decreased even further by $\mathbf{J}_{dia\ \nabla\cdot\overleftrightarrow{T}}$'s impact on the flank mangetopause.

These conclusions are a result of our η-based MP selection process; however, in the initial phase of analyzing the database's magnetopause crossing data, we used the HT time frames in lieu of a more refined magnetopause current sheet boundary. While the HT time frame widely overextends the boundaries of the magnetopause, leading to highly inaccurate current density and current sheet thickness results, it did, however, give us the same competitive relation between the temperature and density diamagnetic components. This indicates that, while current density is highly correlated to the magnetopause current sheet, the fundamental nature of the competition between the two diamagnetic components is intrinsic to magnetosheath - magnetosphere interaction and is thus present whether considering a large swath of the magnetopause, or a more defined magnetopause current sheet layer.

4 Discussion

4.1 Physical Interpretations

We have found that the ion temperature and density components actively compete with one another, resulting in a weaker total diamagnetic current and current asymmetries across the magnetopause.

These observations are generally consistent with previously literature regarding ion populations in the magnetosphere. From Chappell et al. (2008), the warm plasma cloak is defined as a population of 10 eV to 3 keV ions energized in the polar cap and magnetotail, which circulates in a dawn-to-dusk circulation pattern throughout the inner magnetosphere out to the magnetopause. As Chappell et al. (2008) notes, the warm plasma cloak ions can occupy the same space as the much warmer and more energetic ring current ions, which circulate in the opposite direction across the magnetosphere, from dusk-to-dawn. Thus it is possible, on a simplified level of magnetospheric circulation, that the colder warm plasma cloak ions provide generating pressure for the density gradient component across the magnetopause in its dawn-to-dusk, CF current like direction, while the warmer ring current ions provide generating pressure for the temperature gradient component in its dusk-to-dawn direction. The density component's dayside-flank asymmetry could also be explained by additional density gradients generated by the plasmasphere drainage plume (Borovsky & Denton, 2008), which exhausts through the dayside magnetopause during storm conditions, enhancing the dayside with more cold ions, thus leading to an enhanced dayside $\mathbf{J}_{dia\ \nabla N}$ while leaving the dusk and dawn components reliant solely on the warm plasma cloak ion population. Additional study regarding the component generation is needed however.

Using these same large scale current properties, we also begin to see the physical formulation of magnetosphere current closure. In static conditions, the parallel current can be described as the divergence of the diamagnetic current, which is, by definition, a perpendicular current. If we then split the total diamagnetic current into its components, we have $\nabla \cdot (\mathbf{J}_{dia\ \nabla N} + \mathbf{J}_{dia\ \nabla \cdot \overleftrightarrow{T}})$. However, as noted earlier, the temperature component does not show a dependence on local time across the magnetopause and, instead, stays almost unchanged on the flanks and dayside. Thus, the temperature component is not likely to have an impact on the parallel current. This is in contrast with the density component which does show a dependence on local time with a stronger dayside than flank current density. This indicates that when concerned with parallel current and current closure with Region I and Region II currents, it is sufficient to make the assumption that the density component is primarily responsible for parallel current generation.

4.2 Large and Small Scale Considerations

Even though the electron diamagnetic current was found to be significant on electron scale current sheets by Shuster et al. (2019, 2021), we found the electron current to be less significant over our ion scale magnetopause current sheets. Specifically the electron diamagnetic current density is 7.8% of the ion diamagnetic current density in the ϕ direction on the dusk, 10.4% on the dayside, and 24.4% on the dawn. This presents an interesting asymmetry for the electron current as it is noticeably weaker on average on the dusk than it is on the dawn; however, in both cases, the electron diamagnetic current is weaker than the contribution made by the ion current. The weaker electron current density may be explained based on the fact that we are averaging over many electron scale current sheets when considering our ion scale magnetopause crossing, thus lowering the resulting current density.

Additionally, while Figure 3 and Table 1 both tell a clear story in the two dimensional $X_{GSE} - Y_{GSE}$ plane, the three dimensional picture is murkier. The θ accumulation component in Figure 3c relates how the currents flow into the Z_{GSE} plane across the magnetopause. The accumulations for $\mathbf{J}_{curl}$ follow the expected directions for the CF current sheet as they go in the $+\theta$ direction on the dusk and on the $-\theta$ on the dawn, relating to a clockwise dawn-to-dusk 3D current system across the magnetopause. However, the diamagnetic currents do not follow such a clear pattern and while $\mathbf{J}_{dia\ Total}$ and $\mathbf{J}_{dia\ \nabla N}$ generally follow $\mathbf{J}_{curl}$ closely for their ϕ components, the same cannot be said for the θ components. As this study stays firmly in the two dimensional realm of the magnetopause current, future studies will need to explore this 3-dimensional picture.

5 Conclusions

Diamagnetic currents play an integral role in the magnetopause; however, the literature has lacked a complete grasp of the temperature gradient's impact on this current system. From our large scale, systematic study of four years of MMS transits, we have quantified this contribution for the first time. Based on our findings, we came to the following conclusions:

1. The temperature gradient component makes up to one-third of the ion diamagnetic current generated along the magnetopause.
2. The temperature gradient moves in the direction opposite to the classical CF current direction, interfering destructively with the density gradient component.
3. The temperature gradient's destructive impact is most pronounced on the flank mangetopause.
4. The total electron diamagnetic current density is weaker than the total ion diamagnetic current on average, equal to 7.8% to 24.2% of the ion current density.

5. Conclusion 2 is insensitive to the precise magnetopause selection process used, indicating that the competitive nature of the temperature and density generated diamagnetic currents is inherent to magnetosheath/magnetosphere interaction and is not limited to what is generally considered to be the magnetopause current sheet.

Therefore temperature gradients in the magnetopause boundary layer impact both the resulting ion current density and fundamentally change the current sheet's structure through its deconstructive relationship with the density component. Future studies will expand on the relation between these two diamagnetic current components and the magnetopause current sheet structure.

Acknowledgments

We thank the team that developed the MMS crossing database created for the International Space Science Institute Team 442, "Study of the physical processes in magnetopause and magnetosheath current sheets using a large MMS database" as well as the entire MMS team and instrument leads for the data access and support. We also thank the pySPEDAS team for their support and data analysis tools. This research was supported by the NASA Magnetospheric Multiscale Mission in association with NASA contract NNG04EB99C. J. M. H. B. and V. M. U. were supported through the cooperative agreement NNG11PL10ANNG11PL10A. The MMS data used in this study is publicly available at https://lasp.colorado.edu/mms/sdc/public/datasets/ from the FPI, FIELDS, and HPCA datasets. The averaged MMS data over the 767 MP crossings identified by and used for this study are available through a Harvard Dataverse public database: https://doi.org/10.7910/DVN/SRBJCR.

References

Borovsky, J. E., & Denton, M. H. (2008). A statistical look at plasmaspheric drainage plumes. *Journal of Geophysical Research: Space Physics*, *113*(A9). doi: 10.1029/2007JA012994

Burch, J. L., Moore, T. E., Torbet, R. B., & Giles, B. L. (2015). Magnetospheric multiscale overview and science objectives. *Space Science Review*, *199*, 5-21. doi: 10.1007/s11214-015-0164-9

Cahill, L. J., & Amazeen, P. G. (1963). The boundary of the geomagnetic field. *Journal of Geophysical Research*, *68*(7), 1835-1843. doi: 10.1029/JZ068i007p01835

Chapman, S., & Ferraro, V. C. A. (1931). A new theory of magnetic storms. *Terrestrial Magnetism and Atmospheric Electricity*, *36*, 77-97.

Chappell, C. R., Huddleston, M. M., Moore, T. E., Giles, B. L., & Delcourt, D. C. (2008). Observations of the warm plasma cloak and an explanation of its formation in the magnetosphere. *Journal of Geophysical Research*, *113*(A09206). doi: 10.1029/2007JA012945

Dong, X. C., Dunlop, M. W., Wang, T. Y., Cao, J. B., Trattner, K. J., Bamford, R., ... Torbert, R. B. (2018). Carriers and sources of magnetopause current: Mms case study. *Journal of Geophysical Research: Space Physics*, *123*, 5464–5475. doi: https://doi.org/10.1029/2018JA025292

Dunlop, M. W., Southwood, D. J., Glassmeier, K.-H., & Neubauer, F. M. (1988). Analysis of multipoint magnetometer data. *Advanced Space Research*, *8*, 273-277.

Fuselier, S. A., Mukherjee, J., M. H. Denton, S. M. P., Trattner, K. J., Toledo-Redondo, S., André, M., ... Burch, J. L. (2019). High-density o^+ in earth's outer magnetosphere and its effect on dayside magnetopause magnetic reconnection. *Journal of Geophysical Research: Space Physics*, *124*(12), 10257–10269. doi: https://doi.org/10.1029/2019JA027396

Ganushkina, N. Y., Liemohn, M. W., & Dubyagin, S. (2018). Current systems in the

earth's magnetosphere. *Reviews of Geophysics*, *56*, 309–332. doi: https://doi.org/10.1002/2017RG000590

Haaland, S., Paschmann, G., Øieroset, M., Phan, T., Hasegawa, H., Fuselier, S. A., ... Burch, J. (2020). Characteristics of the flank magnetopause: Mms results. *Journal of Geophysical Research: Space Physics*, *125*. doi: https://doi.org/10.1029/2019JA027623

Haaland, S., Reistad, J., Tenfjord, P., Gjerloev, J., Maes, L., DeKeyser, J., ... Dorville, N. (2014). Characteristics of the flank magnetopause: Cluster observations. *Journal of Geophysical Research: Space Physics*, *119*, 9019–9037. doi: doi:10.1002/2014JA020539

Haaland, S., Runov, A., Artemyev, A., & Angelopoulos, V. (2019). Characteristics of the flank magnetopause: Themis observations. *Journal of Geophysical Research: Space Physics*, *124*, 3421–3435. doi: https://doi.org/10.1029/2019JA026459

Hasegawa, H. (2012). Structure and dynamics of the magnetopause and its boundary layers. *Monogr. Environ. Earth Planets*, *1*(2), 71-119. doi: 10.5047/meep.2012.00102.0071

Le, G., & Russell, C. T. (1994). The thickness and structure of high beta magnetopause current layer. *Geophysical Research Letters*, *21*(23), 2451-2454. doi: https://doi.org/10.1029/94GL02292

Paschmann, G., Haaland, S. E., Phan, T., Sonnerup, B., Burch, J., Torbert, R., ... Fuselier, S. (2018). Large-scale survey of the structure of the dayside magnetopause by mms. *Journal of Geophysical Research: Space Physics*, *123*, 2018–2033. doi: https://doi.org/10.1002/2017JA025121

Paschmann, G., Sonnerup, B., Haaland, S. E., Phan, T., & Denton, R. E. (2020). Comparison of quality measures for walén relation. *Journal of Geophysical Research: Space Physics*, *125*(e2020JA028044). doi: https://doi.org/10.1029/2020JA028044

Phan, T. D., Larson, D. E., Lin, R. P., McFadden, J. P., Anderson, K. A., Carlson, C. W., ... Szabo, A. (1996). The subsolar magnetosheath and magnetopause for high solar wind ram pressure: Wind observations. *Geophysical Research Letters*, *23*(10), 1279-1282. doi: https://doi.org/10.1029/96GL00845

Phan, T. D., & Paschmann, G. (1996). Low-latitude dayside magnetopause and boundary layer for high magnetic shear: 1. structure and motion. *Journal of Geophysical Research: Space Physics*, *101*(A4), 7801-7815. doi: https://doi.org/10.1029/95JA03752

Pollock, C., Moore, T., Jacques, A., Burch, J., Gliese, U., Saito, Y., ... et al (2016). Fast plasma investigation for magnetospheric multiscale. *Space Science Reviews*, *199*, 331-406. doi: https://doi.org/10.1007/s11214-016-0245-4

Russell, C. T., Anderson, B. J., Baumjohann, W., Bromund, K. R., Dearborn, D., Fischer, D., ... Richter, I. (2016). The magnetospheric multiscale magnetometers. *Space Science Reviews*, *199*, 189-256. doi: https://doi.org/10.1007/s11214-014-0057-3

Shuster, J. R., Gershman, D. J., Chen, L.-J., Wang, S., Bessho, N., Dorelli, J. C., ... Viñas, A. F. (2019). Mms measurements of the vlasov equation: Probing the electron pressure divergence within thin current sheets. *Geophysical Research Letters*, *46*. doi: https://doi.org/10.1029/2019GL083549

Shuster, J. R., Gershman, D. J., Dorelli, J. C., Giles, B. L., Wang, S., Bessho, N., ... Torbert, R. B. (2021). Structures in the terms of the vlasov equation observed at earth's magnetopause. *Nature Physics*. doi: https://doi.org/10.1038/s41567-021-01280-6

Sonnerup, B. U., & Wang, D. J. (1987). Structure of reconnection boundary layers in incompressible mhd. *Journal of Geophysical Research*, *92*(A8), 8621-8633. doi: 10.1029/JA092iA08p08621

Young, D. T., Burch, J. L., Gomez, R. G., Santos, A. D. L., Miller, G. P., IV, P. W.,

... Webster, J. M. (2016). Hot plasma composition analyzer for the magnetospheric multiscale mission. *Space Science Reviews*, *199*, 407-470. doi: https://doi.org/10.1007/s11214-014-0119-6